



Original article

Electrochemical, spectroscopic, and molecular docking studies of the interaction between the anti-retroviral drug indinavir and dsDNA

Fariba Mollarasouli ^{a,b}, Burcu Dogan-Topal ^a, Mehmet Gokhan Caglayan ^a, Tugba Taskin-Tok ^{c,d}, Sibel A. Ozkan ^{a,*}^a Ankara University, Department of Analytical Chemistry, 06560, Ankara, Turkey^b Department of Chemistry, Yasouj University, Yasouj, 75918-74831, Iran^c Department of Chemistry, Gaziantep University, 27310, Gaziantep, Turkey^d Institute of Health Sciences, Department of Bioinformatics and Computational Biology, Gaziantep University, 27310, Gaziantep, Turkey

ARTICLE INFO

Article history:

Received 25 March 2020

Received in revised form

5 August 2020

Accepted 5 August 2020

Available online 10 August 2020

Keywords:

Glassy carbon electrode

Calf thymus double-stranded

deoxyribonucleic acid (ct-dsDNA)

Biosensor

Fluorescence

Molecular docking

ABSTRACT

In this study, an electrochemical DNA biosensor was developed using a straightforward methodology to investigate the interaction of indinavir with calf thymus double-stranded deoxyribonucleic acid (ct-dsDNA) for the first time. The decrease in the oxidation signals of deoxyguanosine (dGuo) and deoxyadenosine (dAdo), measured by differential pulse voltammetry, upon incubation with different concentrations of indinavir can be attributed to the binding mode of indinavir to ct-dsDNA. The currents of the dGuo and dAdo peaks decreased linearly with the concentration of indinavir in the range of 1.0–10.0 µg/mL. The limit of detection and limit of quantification for indinavir were 0.29 and 0.98 µg/mL, respectively, based on the dGuo signal, and 0.23 and 0.78 µg/mL, respectively, based on the dAdo signal. To gain further insights into the interaction mechanism between indinavir and ct-dsDNA, spectroscopic measurements and molecular docking simulations were performed. The binding constant (K_b) between indinavir and ct-dsDNA was calculated to be $1.64 \times 10^8 \text{ M}^{-1}$, based on spectrofluorometric measurements. The obtained results can offer insights into the inhibitory activity of indinavir, which could help to broaden its applications. That is, indinavir can be used to inhibit other mechanisms and/or hallmarks of viral diseases.

© 2020 Xi'an Jiaotong University. Production and hosting by Elsevier B.V. This is an open access article under the CC BY-NC-ND license (<http://creativecommons.org/licenses/by-nc-nd/4.0/>).

1. Introduction

Indinavir (IND), made by Merck under the trading name of Crixivan[®] (Fig. 1), is an anti-retroviral drug acting as a competitive and reversible protease inhibitor, and has an essential role against human immunodeficiency virus infection and acquired immune deficiency syndrome (HIV/AIDS) replication [1]. It is a white powder soluble in water that can be administered orally. It may be used in combination with other medications, such as ritonavir, to boost IND activity during highly active anti-retroviral therapy (HAART) [2]. IND does not affect the early stages of HIV replication; instead, it disrupts the production of infectious HIV, decreasing the contagiousness of the virus [3]. Therefore, IND works better for controlling HIV infection. The mechanism of action of IND depends on the inhibition of the HIV protease, blocking virus maturation and decreasing the

number of reproducing HIV viruses, thus causing a decrease in the viral load and the formation of immature and noninfectious virions. Hence, the immune system can work better. IND can act in both chronically and acutely infected cells, whereas nucleoside reverse transcriptase inhibitors (NRTIs) do not affect chronically infected cells. In commercially available IND, an additional amine in the hydroxy ethylene backbone of the anhydrous form of the drug is added to enhance solubility and oral bioavailability, facilitating drug intake. In vitro studies have shown that the antiviral effects of HIV protease inhibitors and those of non-nucleoside reverse transcriptase inhibitors (NNRTIs) or some NRTIs might be additive or synergistic [3]. IND can be detected in the cerebrospinal fluid of a person who is administered the drug. Over a concentration range of 0.05–10 mg/mL, approximately 60% of IND can bind to proteins. IND is mainly metabolized by the liver and is rapidly absorbed, reaching its highest plasma concentration within 0.8 ± 0.3 h. The average plasma half-life of IND is 1.8 h for adults and 1.1 h for children [3].

Several techniques, including UV absorbance measurements [4], high-performance liquid-chromatography (HPLC), electrochemistry [5–7], capillary electrophoresis [8], and liquid-chromatography-

Peer review under responsibility of Xi'an Jiaotong University.

* Corresponding author.

E-mail address: ozkan@pharmacy.ankara.edu.tr (S.A. Ozkan).

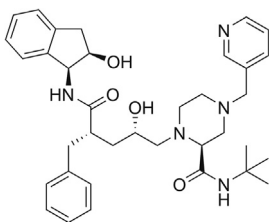


Fig. 1. The structure of indinavir.

tandem mass spectroscopy (LC-MS/MS) [9], have been used for IND detection. However, the availability of time- and cost-saving methods that can detect IND with high sensitivity opens new possibilities for the future of pharmaceutical analysis. Electrochemistry offers such advantages. In a study conducted by Dogan et al. [6] in 2006, the behavior of IND subjected to electrochemical reduction was investigated. The results indicated a diffusion controlled process, based on the IND peak. The limit of detection (LOD) was determined to be as low as 1.26×10^{-7} M [6]. To the best of our knowledge, the interaction between IND and dsDNA has not been studied by any method. The study of the drug-DNA interaction using electrochemistry can be used not only to understand the mechanism of drug action and to design new and more efficient drugs, but also to determine the specific drug compounds.

DNA exists in the form of a double helix, consisting of two strands composed of four types of nucleobase subunits: guanine (G), cytosine (C), adenine (A), and thymine (T) [10]. The two strands are held together mainly through Watson Crick hydrogen bonds, with C-G pairs linked with three hydrogen bonds, and A-T pairs with two hydrogen bonds [11].

DNA replication and transcription are two major cell functions. DNA transcription is required for gene expression and protein synthesis, and therefore, plays key roles in health and disease. Some small organic molecules can mimic signaling regulatory proteins in terms of binding strength and specificity. Consequently, these molecules can activate DNA replication and/or transcription, and increase protein production. On the contrary, other small organic molecules can inhibit DNA-related processes, restricting DNA replication and protein synthesis, leading to cell apoptosis. In most cases, DNA-targeted drugs for antibiotic and antitumor applications are designed to inhibit DNA-related processes, leading to cell apoptosis. Small organic molecules can interact with DNA through groove binding, intercalation, and/or cross-linking (covalent bonding). Complex formation between small organic molecules and DNA through covalent binding or non-covalent interactions results in changes in the functional properties and thermal stability of DNA [12]. Often, such changes have a great impact on physiological functions. Therefore, it is critical to understand the mechanisms underlying small molecule binding to DNA and to elucidate the functional properties of the resulting complexes, which may have applications for drug research and development [13].

Small organic molecules can bind at either the minor or major groove of DNA. The minor and major grooves are a result of the helical structure of the DNA. The glycosidic bonds in the two DNA strands are always in the same location within a base pair, and they are neither parallel nor perpendicular to one another. This asymmetric positioning of the glycosidic bonds creates the major groove at the side where the backbones of the two DNA strands are far apart, and the minor groove at the opposite site, where the backbones of the two strands come close together. In general, groove binding, contrary to intercalation, occurs in two steps. During the first step, the binding molecule undergoes a hydrophobic transfer from the

solution to the groove of DNA. During the second step, the binding molecule forms non-covalent interactions with the DNA nucleobases. Groove binding does not require unwinding of the DNA helical axis. Typically, groove binders prefer to bind at AT-rich sequences because GC-rich sequences contain a $-NH_2$ group that sterically inhibits binding [12,13].

In this study, the interaction of IND with calf thymus double-stranded DNA (ct-dsDNA) was investigated with a glassy carbon electrode (GCE) modified with a multilayer of ct-dsDNA. The results were confirmed by three independent techniques, namely, electrochemical and fluorescence measurements, and molecular modeling.

2. Experimental

2.1. Apparatus and software

Electrochemical measurements were performed with an AUTOLAB PGSTAT 30 potentiostat/galvanostat (Eco Chemie, the Netherlands), equipped with a three-electrode cell system and running the GPES 4.9 software. The three-electrode system consisted of an Ag/AgCl electrode (BASi; 3 M NaCl) as the reference electrode, a bare and modified GCE as the working electrode ($\varphi = 3.0$ mm for the unmodified electrode shipped from BASi), and a platinum counter electrode. The pH was adjusted using a digital pH meter Model 538 (WTW, Austria), equipped with a combined glass electrode. UV-vis absorption spectra were recorded on the Agilent Cary 60 UV-Vis Spectrophotometer. Spectrofluorometric measurements were conducted on the Agilent Cary Eclipse Fluorescence Spectrophotometer, using a quartz fluorescence cuvette (10 mm \times 10 mm).

2.2. Reagents and solutions

Indinavir sulfate (IND) was kindly provided by Merck Sharp & Dohme Pharm. Ind. (Istanbul, Turkey). An IND stock solution (1000 μ g/mL) was prepared by dissolving the powder in ultrapure water and was stored in the refrigerator. Acetic acid, sodium acetate, and methylene blue were purchased from Merck. Calf thymus double-stranded DNA (ct-dsDNA) was purchased from Sigma (D1501), and was used for studying its interaction with IND. The stock solution of ct-dsDNA (500 μ g/mL) was prepared in ultrapure water from a Millipore Milli-Q system and stored at 4 $^{\circ}$ C overnight. Further required dilutions of the ct-dsDNA stock solution were prepared in ultrapure water. Acetate buffer was prepared by mixing 0.1 M sodium acetate and 0.1 M acetic acid solutions. The concentration of the ct-dsDNA stock solution was determined by UV absorption measurements at 260 nm according to Lambert - Beer's Law equation, $A = \epsilon bc$, where A represents the absorption value, ϵ is the molar absorption coefficient ($\epsilon_{260} = 6600$ L/mol/cm), b is the cuvette path length (1 cm), and c represents the drug concentration. To evaluate the purity of ct-dsDNA, the ratio of the absorbance at 260 nm to the absorbance at 280 nm (A_{260}/A_{280}) was calculated, and if it was higher than 1.8, it could be concluded that the ct-dsDNA preparation was sufficiently protein-free [14]. All chemicals used were of analytical reagent grade, and their solutions were prepared by using double distilled water.

2.3. Electrochemical measurements

Differential pulse (DP) voltammograms were recorded from 0.2 to 1.5 V vs. Ag/AgCl (3 M NaCl), using the following parameters: pulse amplitude = 50 mV, pulse time = 70 m s, and scan rate = 5 mV/s. For the incubation in the solution phase, a mixture solution was prepared by mixing 100 μ g/mL ct-dsDNA with 10 μ g/

mL IND in 0.1 M acetate buffer (pH = 4.70), and then, incubated for different periods of time at room temperature. To calculate the binding constant, increasing concentrations of ct-dsDNA (4.83×10^{-6} – 1.60×10^{-5} M) were added to a fixed concentration of IND in solution.

To fabricate the DNA biosensor, the surface of the cleaned GCE was coated by drop-casting with 5 μ L of 50 μ g/mL ct-dsDNA (prepared freshly), followed by drying in an oven for 10 min at 45 °C. This step was repeated three times for each biosensor. Finally, the prepared DNA biosensor was cleaned by immersion into a blank acetate buffer solution for 1 s to remove the unbound ct-dsDNA from the electrode surface. The ct-dsDNA-modified biosensor was immersed in an IND solution, and was incubated for different time periods. Then, the biosensor was cleaned again with blank acetate buffer solution for 5 s to remove any unbound IND [15]. DP voltammograms were recorded in a cleaned blank acetate buffer solution (0.1 M, pH = 4.70) in the range of 0.2 and 1.5 V vs. Ag/AgCl (3 M NaCl). Each experiment was performed with a new biosensor.

2.4. Fluorescence measurements

Fluorescence spectra of methylene blue (MB) at a concentration of 5.0 μ M were recorded in the absence or presence of different ct-dsDNA concentrations with a spectrofluorometer using the following parameters: excitation wavelength = 290 nm, excitation and emission slits = 10 nm, photomultiplier tube voltage = 675 V. The fluorescence spectra were recorded continually while adding dropwise small volumes (1 μ L) of a stock solution of 1.92 mM ct-dsDNA to a 50 μ M aqueous solution of MB under stirring. Fluorescence measurements at different temperatures were recorded after waiting 3 min at each temperature to reach equilibrium. Millipore Milli-Q water was used as a blank solution. Progressive quenching of the MB fluorescence signal was observed at increasing DNA concentrations, indicating an interaction between MB and ct-dsDNA. It was assumed that the observed fluorescence quenching could be attributed to the formation of a fluorophore-quencher complex. When the MB fluorescence signal did not change with the further addition of ct-dsDNA, we started to add small volumes (1 μ L) of a stock solution of 5 mM IND to the fluorophore-quencher complex solution. In this case, the MB fluorescence signal was recovered because of the stronger DNA binding properties of IND compared to MB, which resulted in the displacement of MB from the MB-DNA complex. This process was continued until a constant fluorescence signal for MB was reached. All fluorescence experiments were repeated at different temperatures (297 K, 301 K, 305 K, and 311 K) adjusted by a Peltier temperature controller.

2.5. Molecular modeling study

Molecular docking with IND as the ligand and DNA as the target was performed using the Discovery Studio (DS) 2019 software suite [16] to investigate and visualize the interaction mechanisms and the possible orientations of the complex. The crystal structure of DNA (ID: 1BNA) [17] was uploaded from the protein data bank, PDB (<http://www.rcsb.org/pdb>). Additionally, the three dimensional (3D) coordinates of IND were optimized at DFT/B3LYP/6-31G × level by using the Gaussian 09 (G09) software [18]. The optimized IND structure and all related information are given in Fig. S1 and Table S1. The target (DNA) was also minimized with the 'prepare protein' protocol of DS 2019 [16]. This protocol uses the CHARMM force field and the adopted-basis Newton-Raphson (ABNR) method [19] to prepare the target for molecular docking. At the end of the docking simulations, the best IND conformer was selected from 50 diversified conformers, based on high negative

values of the calculated binding energy, three-dimensional interaction types, and the lowest values of root mean square deviation (RMSD), using DS 2019 [16].

3. Results and discussion

3.1. Electrochemical studies of the IND-ct-dsDNA interaction

As seen in Fig. 2, the DP voltammograms of 10 μ g/mL IND in 0.1 M acetate buffer solution (pH = 4.70) in the potential range of 0.2–1.5 V vs. Ag/AgCl (3 M NaCl) show one oxidation peak at a potential of 0.80 V.

The molecular structure of IND reveals the presence of a piperazine ring in Ref. [24], which is a basic center that, owing to its available non-bonding electrons, can act as a donor. Therefore, it can be assumed that the main oxidation step of IND should occur on the piperazine ring. According to the literature, a nitrogen on the piperazine ring loses an electron to form a cation radical, which, in subsequent steps, loses a proton and an electron to form a quaternary Schiff base [25–27].

The DP voltammograms of the biosensor-attached DNA at the same electrolyte displayed two oxidation peaks, attributed to the oxidation of dGuo at 0.96 V and that of dAdo at 1.23 V vs. Ag/AgCl (3 M NaCl). It is clear from Fig. 2 that no changes were observed when the DNA biosensor was incubated in the 0.1 M acetate buffer solution (pH = 4.70) without the addition of the IND drug. On the contrary, a significant decrease in the current of the dGuo and dAdo peaks, along with a positive shift in the dGuo oxidation peak potential, was observed after incubating the DNA biosensor in a 0.1 M acetate buffer solution (pH = 4.70) containing the IND drug, indicating possible interactions between IND and ct-dsDNA.

3.1.1. In-solution phase

The interaction of IND with ct-dsDNA was investigated by DP voltammetry (DPV) in the solution phase, after different incubation times. From preliminary DPV measurements, it was observed that in the solution phase, the DPV peak current of 10 μ g/mL IND decreased just after mixing with 100 μ g/mL of ct-dsDNA (Fig. 3A).

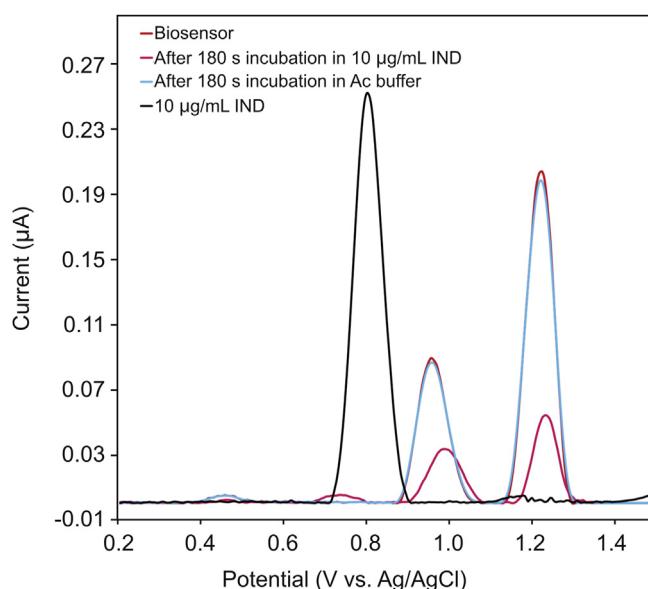


Fig. 2. DP voltammograms of 10.0 μ g/mL IND, the ct-dsDNA biosensor, the ct-dsDNA biosensor after incubation in bare 0.1 M acetate buffer (pH = 4.7), and the ct-dsDNA biosensor after incubation in 10.0 μ g/mL IND; Pulse amplitude = 50 mV, pulse time = 70 ms, and scan rate = 5 mV/s.

Moreover, a similar decrease in the current of the dGuo peak was observed in the mixture solution of IND and ct-dsDNA compared to a solution of 100 µg/mL of ct-dsDNA in the absence of IND. This decrease in the current of the IND and dGuo peaks can be explained from a reduction in the equilibrium concentration of free IND and ct-dsDNA [28].

Hence, the incubation of IND with ct-dsDNA in the solution phase was monitored by recording the DPV signal of a mixture of 10 µg/mL IND and 100 µg/mL of ct-dsDNA prepared in a 0.1 M of acetate buffer solution (pH = 4.70) at room temperature, after different incubation time periods, ranging from 0 to 240 min. The DP voltammogram of only 100 µg/mL ct-dsDNA solution was recorded to control the IND–ct-dsDNA interaction. As can be seen in Fig. 3B, with increasing incubation time, the current of the IND peak at approximately 0.8 V and of the dGuo peak at approximately 0.96 V gradually decreased, accompanied with a positive shift in the peak potential of IND and dGuo, which is consistent with the results from the DNA biosensor (Section 3.1.2). It should be noted that the surface of the GCE should be polished after each measurement to remove any electro-active contaminants adsorbed on its surface, which can block the

electrode surface.

3.1.2. In-situ study using the ct-dsDNA-electrochemical biosensor

Incubation time is an important parameter for the interaction of IND with the ct-dsDNA-coated GCE surface; hence, its optimization is necessary. In order to obtain the optimum interaction time, the oxidation signals of the ct-dsDNA biosensor were measured in the absence and presence of 10 µg/mL IND after different incubation times, in the range of 30–300 s. Fig. 4A shows the DP voltammograms and currents of the dGuo and dAdo peaks for ct-dsDNA as a function of interaction time with IND. As can be seen from Fig. 4B, a significant decrease in the current of the dGuo and dAdo peaks was observed as the incubation time increased up to 180 s, followed by an increase in the ct-dsDNA signal after 300 s of interaction time. Therefore, an incubation time of 180 s was selected for all of the subsequent experiments. The value of the percentage of dGuo signal change (S%) is one way to interpret the interaction between ct-dsDNA and IND. This value was calculated for each incubation time based on the equation described by Carter et al. [29]:

$$S\% = \frac{S_s}{S_b} \times 100 \quad (1)$$

where S_s and S_b are the dGuo oxidation signals after and before the interaction, respectively. S% values for all incubation times (30, 60, 120, 180, and 300 s) were obtained using equation (1), and are shown in Table S2. According to the literature, if a sample has an S% value higher than 85%, it is considered non-toxic, whereas if the S% value is less 50%, it is considered toxic. When the S% value lies between 50 and 85, it is classified as a moderately poisonous sample [29–31].

According to this theory, IND does not have any toxic effect on ct-dsDNA when the incubation time is 180 s. However, it appears to be moderately toxic following shorter incubation times. The toxicity effect of IND was decreased by increasing the interaction time from 30 s to 180 s.

The electrochemical determination of IND was performed by the DPV technique at the ct-dsDNA/GCE biosensor. Fig. 5A shows typical DP voltammograms of the ct-dsDNA-coated GCE when incubated with various IND concentrations in the range of 0.0–10.0 µg/mL in the 0.1 M acetate buffer solution (pH = 4.70). The current of the dGuo and dAdo peak was decreased with increasing IND concentration, which could be ascribed to the binding of IND to ct-dsDNA on the GCE surface. This decrease in the dGuo and dAdo peak currents can be explained as possible damage of the oxidizable groups in the electroactive bases of ct-dsDNA at the GCE surface due to interactions with IND [32]. The presence of a positive or negative shift in the dGuo oxidation peak potential is considered to be an indication of the binding mode, intercalation or electrostatic, respectively [28,33]. As can be seen from Fig. 5B, IND addition caused a positive shift in the oxidation peak potential of dGuo, suggesting that the interaction between IND and ct-dsDNA occurs through groove binding or poor intercalation. In addition, the relationship between the current of the oxidation peaks for dGuo and dAdo and the IND concentration in the range of 0.0–10.0 µg/mL can be described well with the following linear equations: I (µA) = -0.0054 [IND] + 0.0842 ($R^2 = 0.9908$) for dGuo, and I (µA) = -0.0145 [IND] + 0.2024 ($R^2 = 0.9909$) for dAdo. The IND LOD and limit of quantification (LOQ) were calculated using the equations $LOD = 3 \text{ s/m}$ and $LOQ = 10 \text{ s/m}$, in which s is the standard deviation for measurements in the absence of IND ($n = 3$), and m is the slope of the calibration plot. Using these equations and the calibration curves, the LOD and LOQ values for IND were found to be 0.29 and 0.98 µg/mL, respectively, based on the dGuo signal, and 0.23 and 0.78 µg/mL, respectively, based on the dAdo signal.

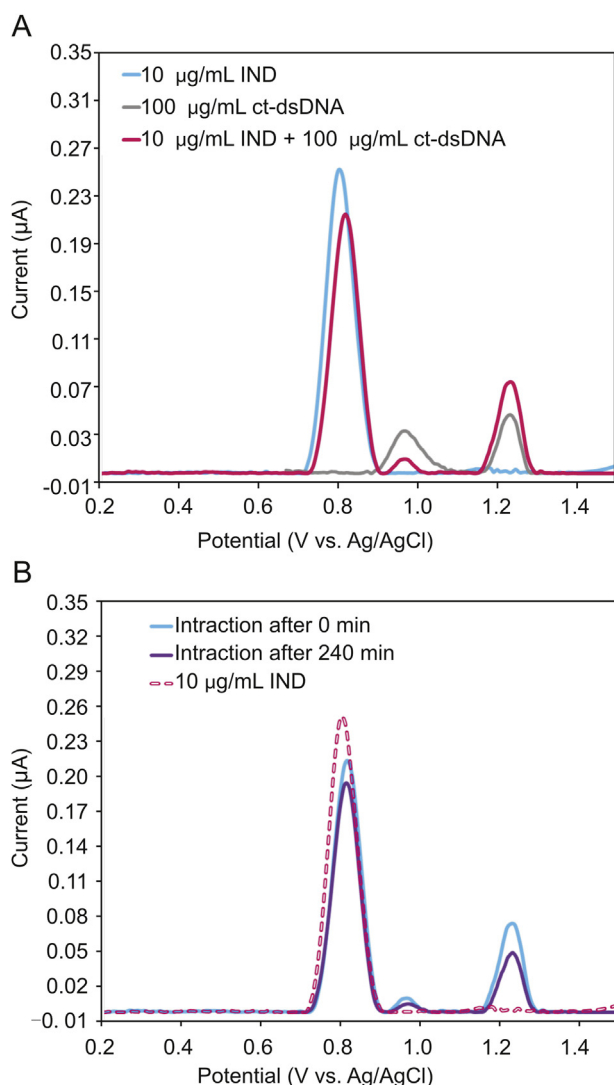


Fig. 3. (A) DP voltammograms of 10 µg/mL IND, 100 µg/mL ct-dsDNA, and of a mixture of 10.0 µg/mL IND with ct-dsDNA, in the solution phase using bare GCE; (B) DP voltammograms of 10 µg/mL IND and its interactions with ct-dsDNA in the solution phase, after an incubation time of 0 min or 240 min, using bare GCE.

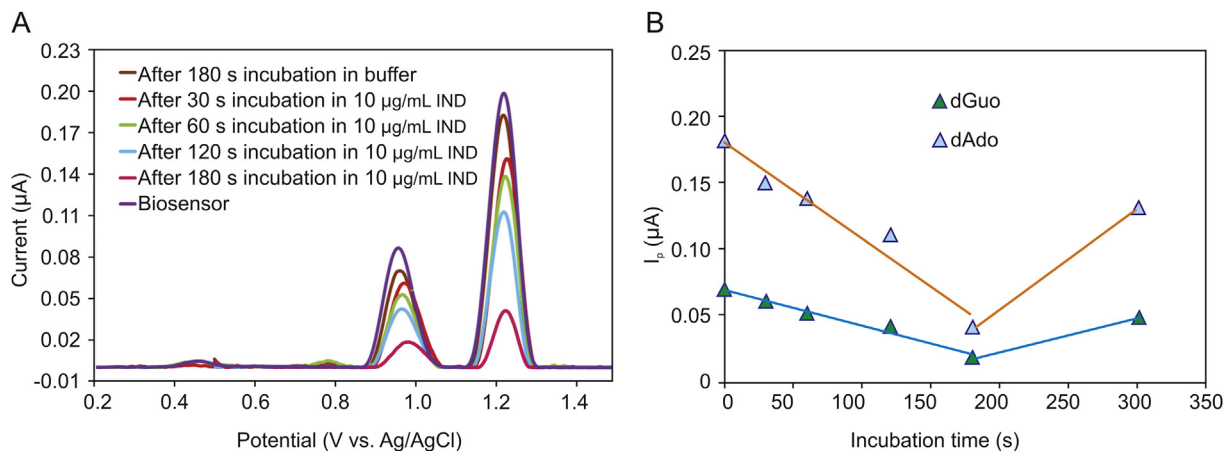


Fig. 4. (A) DPV voltammograms and (B) the plot of the current of the dGuo and dAdo peaks versus incubation time for the interaction of ct-dsDNA biosensor with 10 µg/mL IND for different incubation times (30 s, 60 s, 120 s, 180 s and 300 s).

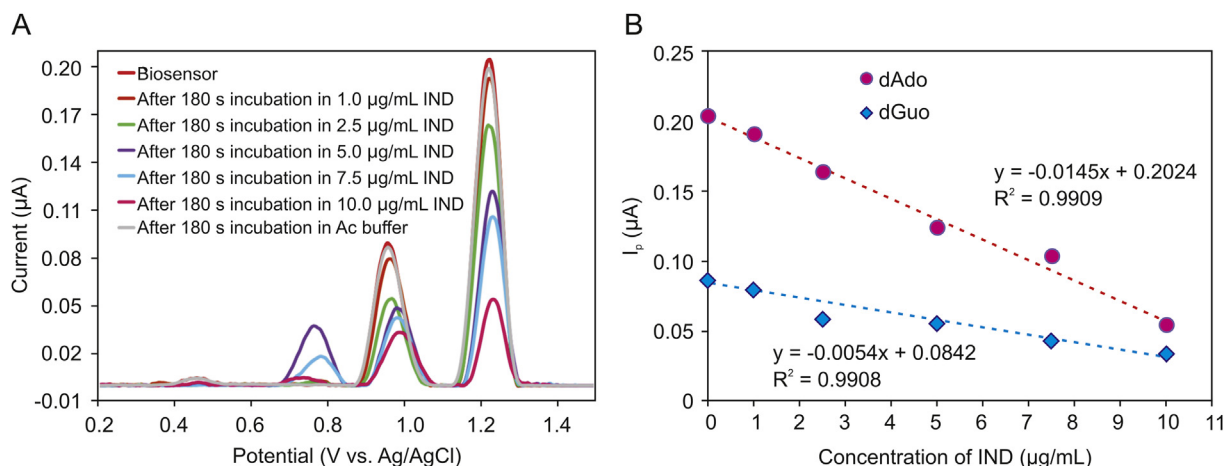


Fig. 5. (A) DPV voltammograms of the ct-dsDNA biosensor after interacting with various IND concentration (1.0, 2.5, 5.0, 7.5, and 10.0 µg/mL) (incubation time: 180 s), (B) Calibration plot for IND determination based on the currents of the dGuo and dAdo peaks.

Analytical figures of merits for the proposed method compared with other methods reported for this drug are given in Table 1. Repeatability and reproducibility parameters were also determined to assess the precision of the method. The repeatability of the measurements conducted with the ct-dsDNA-modified GCE was determined by measuring repeatedly the current of the oxidation peak of dGuo by DVP using the same electrode. The relative standard deviation (RSD) for the three measurements was 1.60%. The reproducibility of the measurements conducted with the ct-dsDNA-modified GCE was evaluated by measuring the current of the oxidation peak of dGuo with five different electrodes. The RSD for the reproducibility study was 2.16%. These results show the excellent performance and precision of the proposed ct-dsDNA-

modified GCE biosensor for the determination of IND.

3.2. Investigation of the interactions between IND and ct-dsDNA using fluorescence spectroscopy

Fluorescence titrations were conducted using the indicator displacement approach. In this competitive approach, the fluorescence signal of the indicator is first quenched by the host molecule. Upon addition of a molecule with a higher affinity toward the host than the indicator, fluorescence recovery occurs owing to the replacement of the indicator. In our study, MB was used as the indicator: MB fluorescence was quenched and red-shifted upon DNA binding (intercalative interaction) (Fig. S2A), and recovered

Table 1

Comparison of the characteristics of the proposed method with other reported methods for quantitative determination of indinavir.

Method	LOD (µg/mL)	LOQ (µg/mL)	Linearity range (µg/mL)	Reference
DPV using HMDE	0.89×10^{-1}	0.30	0.57–5.70	[6]
UV spectrophotometric	14.42	43.69	20.0–80.0	[4]
Capillary electrophoresis	4.61	14.0	20.0–100.0	[8]
LC-MS/MS	–	0.003	0.003–12.32	[9]
ct-dsDNA-IND interaction	0.23	0.78	1.0–10.0	This work

HMDE: Hanging Mercury Drop Electrode.

(fluorescence ON state) when IND interacted with DNA and replaced MB (Fig. S2B).

The indicator displacement assay was performed at four different temperatures to investigate the thermodynamic parameters of the IND-DNA interaction. The binding constant describing the interaction between MB and DNA was calculated using the Stern Volmer equation:

$$\frac{F_0}{F} = 1 + K_q \tau_0 [DNA] = 1 + K_{SV} [DNA] \quad (2)$$

where F and F_0 are the fluorescence intensities in the presence and absence of DNA, respectively, τ_0 is the lifetime of MB fluorescence in the absence of a DNA, K_q is the MB fluorescence quenching rate constant, K_{SV} is the Stern-Volmer constant, and $[DNA]$ is the concentration of DNA (quencher) [34].

The slope of the plot of F_0/F vs. $[DNA]$ gives the Stern-Volmer constant, which, for the MB-DNA interactions, was at the level of $\sim 10^4$. Following that determination, the IND titration data were evaluated using algorithms specific for the indicator displacement assay [35]. The scripts implementing the algorithms were written in Origin C, and the binding constants were calculated using non-linear regression (Fig. 6). The simplest reaction describing the interactions taking place during the indicator displacement assay is:



where DNA-MB is the complex between DNA and MB, DNA-IND is the complex between DNA and IND and MB represents free MB. The algorithms for the data analysis were derived based on the following binding and mass-balance equations:



$$K_i = [DNA-MB]/([DNA][MB]) \quad (6)$$

$$K_b = [DNA-IND]/([DNA][IND]) \quad (7)$$

$$[DNA]_t = [DNA] + [DNA-IND] + [DNA-MB] \quad (8)$$

$$[IND]_t = [IND] + [DNA-IND] \quad (9)$$

$$[MB]_t = [MB] + [DNA-MB] \quad (10)$$

where K_b is the binding constant for the interaction between IND and DNA, K_i is the binding constant for the interaction between MB and DNA, $[DNA]_t$ is the total DNA concentration, $[IND]_t$ is the total IND concentration, and $[MB]_t$ is the total MB concentration. Based on the above assumptions, the following equations were derived for the solution:

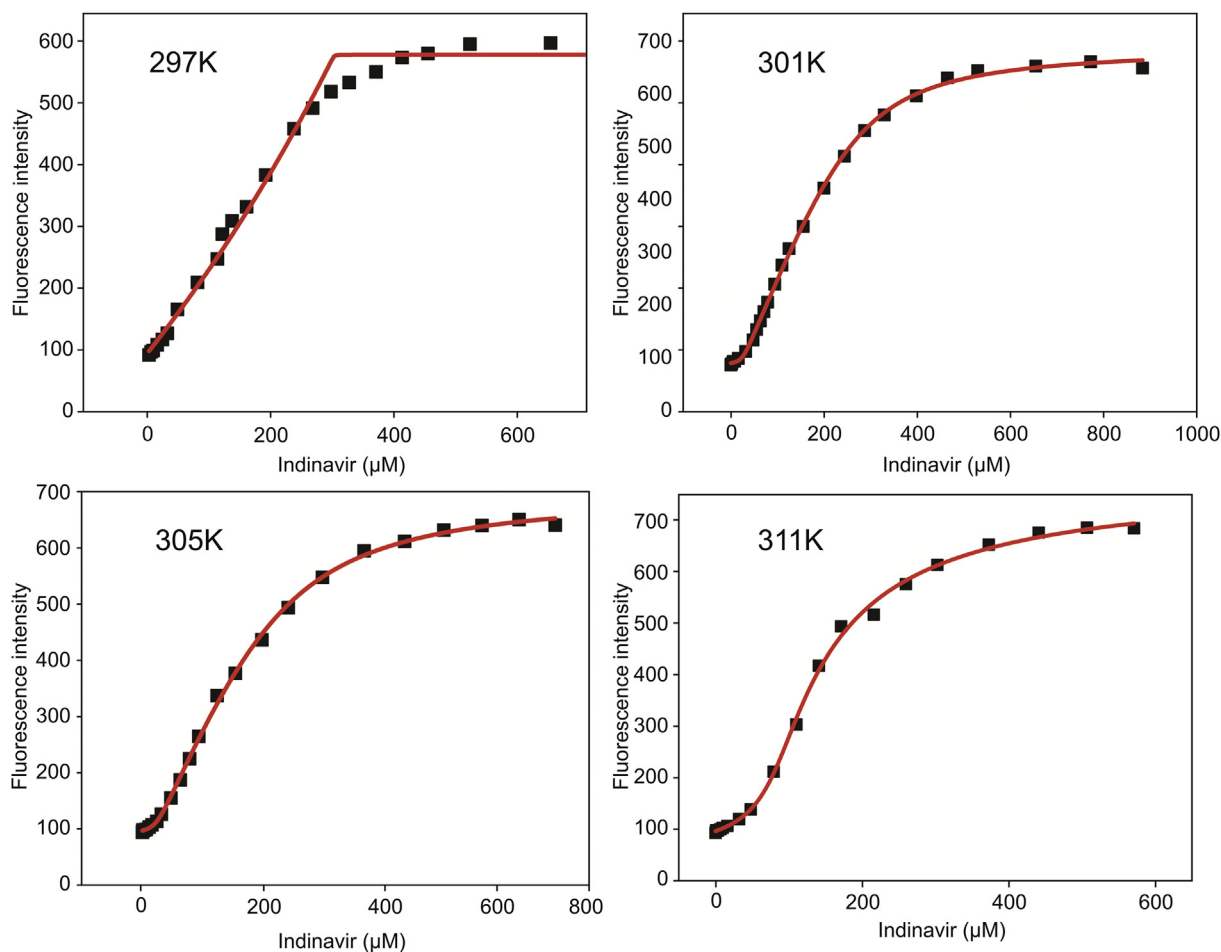


Fig. 6. IND–MB + DNA titration isotherms and non-linear regression for binding constant calculations at different temperatures.

Table 2
Thermodynamic parameters for indinavir-DNA interaction calculated using fluorescence titrations.

Temperature	K_b (M^{-1})	ΔG° (kcal/mol)	ΔS° (cal/K/mol)	ΔH° (kcal/mol)
297 K	1.64×10^8	-2.86	-39.0	-14.5
301 K	6.04×10^7	-2.70		
305 K	1.94×10^7	-2.54		
311 K	2.14×10^6	-2.31		

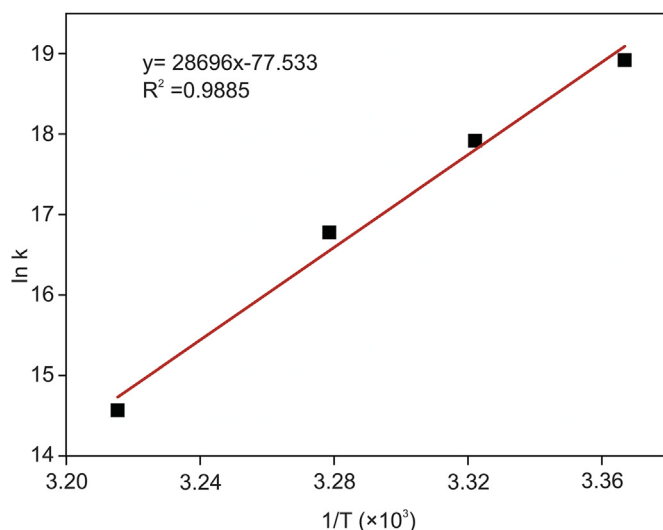


Fig. 7. Van't Hoff plot for the IND-DNA interaction.

$$[DNA - IND] = \frac{K_b [DNA]}{1 + K_b [DNA]} [IND]_t \quad (11)$$

$$[DNA - MB] = \frac{K_i [DNA]}{1 + K_i [DNA]} [MB]_t \quad (12)$$

$$[MB] = \frac{[MB]_t}{1 + K_i [DNA]} \quad (13)$$

and finally, substituting equations (11) and (12) into equation (13):

$$[DNA]_t = [IND] + \frac{K_b [DNA]}{1 + K_b [DNA]} [IND]_t + \frac{K_i [DNA]}{1 + K_i [DNA]} [MB]_t \quad (14)$$

The above algorithms, which were mainly derived from Chaires

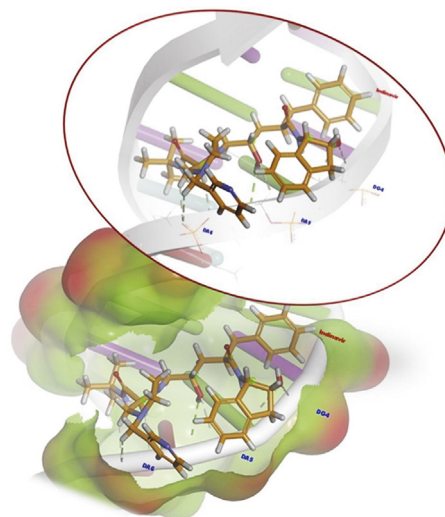


Fig. 8. Global minimum energy binding conformations and interactions of IND in the binding site of DNA.

et al.'s study [35], were then implemented into the relevant scripts. After defining the known values and using a set of initial estimates for the unknown parameters, the solution was computed using Newton's method. Iterations were continued until the non-linear regression converged into a solution.

The binding constants for the IND-DNA interaction were much higher than those for the MB-DNA interaction (Table 2). Finally, binding constants computed at different temperatures were used for constructing a van't Hoff plot (Fig. 7) to derive thermodynamic parameters. Table 2 shows that the Gibbs free energy changes were negative, confirming that the interaction between IND and DNA is spontaneous. The strength of IND binding to DNA (binding constants) decreased with increasing temperature, suggesting that the process is exothermic, which is also supported by the values of enthalpy changes.

Table 3 describes the affinities and modes of binding of some drugs to DNA [20–23,36–38]. Whereas other antiviral drugs, such as lamivudine, ribavirin, and oseltamivir, show weak or moderate binding affinities, IND interacts strongly with DNA, forming eight hydrogen bonds, as revealed in our docking study. Netropsin and diminazene have higher affinities than IND, whereas daunomycin and gemcitabine have weaker binding affinities than IND.

Table 3
DNA binding constants of some drugs at room temperature.

Drug	DNA binding constant (M^{-1})	Proposed binding mode	Reference
Lamivudine	1.3×10^5	Groove binding	[32]
Ribavirin	4.3×10^3	Groove binding	[33]
Oseltamivir	1.8×10^4	Intercalation	[34]
Daunomycin	7.0×10^5	Intercalation	[20]
Netropsin	2.8×10^8	Groove binding	[21]
Diminazene	8.8×10^8	Groove binding	[22]
Gemcitabine	2.0×10^6	Groove binding	[23]
Indinavir	1.6×10^8	Groove binding	This study

3.3. Molecular modeling study of the interaction of IND with ct-dsDNA

Based on the docking results, the calculated binding energy ΔG (kcal/mol) and inhibition constant K_i (nM) for the interaction between IND with DNA were -8.38 kcal/mol and 726.14 nM at 298.15 K, respectively. The docking simulation generated an IND conformation inside the binding pocket of DNA with a binding energy of -8.38 kcal/mol (Fig. 8). All docking solutions were examined in order to select the right conformation. Furthermore, visualization of the interaction between IND and DNA in the complex showed that all of IND structures could enter the DNA binding grooves (Fig. 8). The interactions between IND and DNA were mediated by eight hydrogen bonds, the first two of which were conventional hydrogen bonds; the residues involved were carbon and hydrogen, and bonds were formed with the A:DG4, A:DA5, and A:DA6 nucleotides of the DNA molecules, as shown in Fig. 8 and Table S3.

4. Conclusions

In this study, an electrochemical DNA biosensor based on ct-dsDNA-modified GCE was developed for the detection of IND for the first time. The interaction of IND with ct-dsDNA was confirmed by a decrease in the dGuo and dAdo oxidation peaks. The type of interaction between IND and ct-dsDNA was examined by electrochemical, spectrofluorometric, and modeling approaches. All results suggest that the possible binding mode of IND to ct-dsDNA is based on groove binding via hydrogen bonds. The proposed electrochemical DNA biosensor is simple and sensitive for the determination of IND and possesses a low LOD. Furthermore, the developed sensing platform is a promising candidate for monitoring new dsDNA-drug interactions in pharmaceutical analysis.

Declaration of competing interest

The authors declare that there are no conflicts of interest.

Acknowledgments

F. M. kindly acknowledges the TUBITAK for Program 2221. F.M., B.D.T., M.G.C. and S.A.O thanks for the support of Ankara University. IND was kindly supplied by Merck Sharp & Dohme Pharm. Ind. (Istanbul, Turkey) and we are thankful to them for their support.

Appendix A. Supplementary data

Supplementary data to this article can be found online at <https://doi.org/10.1016/j.jpha.2020.08.004>.

References

- [1] X. Duval, G. Peytavin, I. Albert, et al., Determination of indinavir and nelfinavir trough plasma concentration efficacy thresholds according to virological response in HIV-infected patients, *HIV Med.* 5 (2004) 307–313.
- [2] J. Ray, E. Pang, D. Carey, Simultaneous determination of indinavir, ritonavir and lopinavir (ABT 378) in human plasma by high-performance liquid chromatography, *J. Chromatogr. B* 775 (2002) 225–230.
- [3] T.M. Gonçalves, B.X.F. Pires, D.C.G. Bedor, et al., Determination of indinavir in human plasma and its use in pharmacokinetic study, *Rev. Bras. Ciências Farm.* 43 (2007) 639–647.
- [4] B.H. Rathod, S.S. Rani, N. Kartheek, et al., UV spectrophotometric method development and validation for the quantitative estimation of indinavir sulphate in capsules, *Int. J. Pharm. Pharmaceut. Sci.* 6 (2014) 598–601.
- [5] U. Feleni, U. Sidwaba, H. Makelane, et al., Core-shell palladium telluride quantum dot-hemethiolate cytochrome based biosensor for detecting indinavir drug, *J. Nanosci. Nanotechnol.* 19 (2019) 7974–7981.
- [6] B. Dogan, D. Canbaz, S.A. Ozkan, et al., Electrochemical methods for determination of the protease inhibitor indinavir sulfate in pharmaceuticals and human serum, *Die Pharm. Int. J. Pharm. Sci.* 61 (2006) 409–413.
- [7] E. Dailly, F. Raffi, P. Jolliet, Determination of atazanavir and other antiretroviral drugs (indinavir, amprenavir, nelfinavir and its active metabolite M8, saquinavir, ritonavir, lopinavir, nevirapine and efavirenz) plasma levels by high performance liquid chromatography with UV detecti, *J. Chromatogr. B* 813 (2004) 353–358.
- [8] M.S.A. Prado, E.R.M. Kedor-Hackmann, M.I.R.M. Santoro, et al., Capillary electrophoretic method for determination of protease inhibitor indinavir sulfate used in human immunodeficiency virus therapy, *J. Pharmaceut. Biomed. Anal.* 34 (2004) 441–450.
- [9] A.L. Jayewardene, B. Kearney, J.A. Stone, et al., An LC-MS-MS method for the determination of indinavir, an HIV-1 protease inhibitor, in human plasma, *J. Pharmaceut. Biomed. Anal.* 25 (2001) 309–317.
- [10] S. Bi, B. Pang, T. Zhao, et al., Binding characteristics of salbutamol with DNA by spectral methods, *Spectrochim. Acta Part A Mol. Biomol. Spectrosc.* 111 (2013) 182–187.
- [11] Z. Talebpoor, F. Haghghi, M. Taheri, et al., Binding interaction of spherical silver nanoparticles and calf thymus DNA: comprehensive multispectroscopic, molecular docking, and RAPD PCR studies, *J. Mol. Liq.* 289 (2019), 111185.
- [12] P. Doan, D.R.G. Pitter, A. Kocher, et al., A new design strategy and diagnostic to tailor the DNA-binding mechanism of small organic molecules and drugs, *ACS Chem. Biol.* 11 (2016) 3202–3213.
- [13] P. Doan, Investigating the DNA-Binding Interactions of Small Organic Molecules Utilizing Ultrafast Nonlinear Spectroscopy, Ph.D. Thesis, University of Michigan, The United State, 2016.
- [14] R. Hajian, T. Guan Huat, Spectrophotometric studies on the thermodynamics of anticancer drug-DNA interactions, *J. Spectrosc.* 2013 (2012) 380352, <https://doi.org/10.1155/2013/380352>.
- [15] B. Dogan-Topal, B. Bozal-Palabiyik, S.A. Ozkan, et al., Investigation of anti-cancer drug lapatinib and its interaction with dsDNA by electrochemical and spectroscopic techniques, *Sensor. Actuator. B Chem.* 194 (2014) 185–194.
- [16] Dassault Systèmes BIOVIA, Discovery Studio 2019, San Diego: Dassault Systèmes, 2016. Retrieved from <https://www.3dsbiovia.com/about/citations-references>.
- [17] F.C. Bernstein, T.F. Koetzle, G.J.B. Williams, et al., The Protein Data Bank: a computer-based archival file for macromolecular structures, *J. Mol. Biol.* 112 (1977) 535–542.
- [18] M.J. Frisch, G.W. Trucks, H.B. Schlegel, et al., Gaussian 09, Revision E.01, Gaussian, Inc., Wallingford, CT, USA, 2009.
- [19] P.K. Chattaraj, S. Giri, S. Duley, Update 2 of: electrophilicity index, *Chem. Rev.* 111 (2011) PR43–PR75.
- [20] Y. Yardim, M. Vandeput, M. Çelebi, et al., A Reduced Graphene Oxide-based Electrochemical DNA Biosensor for the Detection of Interaction between Cisplatin and DNA based on Guanine and Adenine Oxidation Signals, *Electroanalysis* 29 (2017) 1451–1458.
- [21] J.M. Kauffmann, J.C. Vire, G.J. Patriarcho, et al., Voltammetric oxidation of trazodone, *Electrochim. Acta.* 32 (1987) 1159–1162.
- [22] B. Uslu, B. Dogan, S.A. Özkan, et al., Electrochemical behavior of vardenafil on glassy carbon electrode: Determination in tablets and human serum, *Anal. Chim. Acta.* 552 (2005) 127–134.
- [23] O.M. Popa, V.C. Diculescu, Electrochemical and spectrophotometric characterisation of protein kinase inhibitor and anticancer drug danusertib, *Electrochim. Acta.* 112 (2013) 486–492.
- [24] G.A. Tığ, B. Zeybek, Ş. Pekyardımcı, Electrochemical DNA biosensor based on poly (2, 6-pyridinedicarboxylic acid) modified glassy carbon electrode for the determination of anticancer drug gemcitabine, *Talanta* 154 (2016) 312–321.
- [25] G. Bagni, D. Osella, E. Sturchio, et al., Deoxyribonucleic acid (DNA) biosensors for environmental risk assessment and drug studies, *Anal. Chim. Acta* 573 (2006) 81–89.
- [26] E. Eksin, E. Zor, A. Erdem, et al., Electrochemical monitoring of biointeraction by graphene-based material modified pencil graphite electrode, *Biosens. Bioelectron.* 92 (2017) 207–214.
- [27] M. Muti, M. Muti, Electrochemical monitoring of the interaction between anticancer drug and DNA in the presence of antioxidant, *Talanta* 178 (2018) 1033–1039.
- [28] A. Erdem, B. Kosmider, R. Osiecka, et al., Electrochemical genosensing of the interaction between the potential chemotherapeutic agent, cis-bis (3-aminoflavone) dichloroplatinum (II) and DNA in comparison with cis-DDP, *J. Pharmaceut. Biomed. Anal.* 38 (2005) 645–652.
- [29] M.T. Carter, M. Rodriguez, A.J. Bard, Voltammetric studies of the interaction of metal chelates with DNA. 2. Tris-chelated complexes of cobalt (III) and iron (II) with 1, 10-phenanthroline and 2, 2'-bipyridine, *J. Am. Chem. Soc.* 111 (1989) 8901–8911.
- [30] C. Qiao, S. Bi, Y. Sun, et al., Study of interactions of anthraquinones with DNA using ethidium bromide as a fluorescence probe, *Spectrochim. Acta Part A Mol. Biomol. Spectrosc.* 70 (2008) 136–143.
- [31] A.E. Hargrove, Z. Zhong, J.L. Sessler, et al., Algorithms for the determination of binding constants and enantiomeric excess in complex host: guest equilibria using optical measurements, *New J. Chem.* 34 (2010) 348–354.
- [32] N. Shahabadi, M. Maghsudi, M. Mahdavi, et al., Interaction of calf thymus DNA with the antiviral drug lamivudine, *DNA Cell Biol.* 31 (2012) 122–127.
- [33] N. Shahabadi, Z.M. Kalar, A. Vaisi-Raygani, DNA interaction studies of an antiviral drug, ribavirin, using different instrumental methods, *DNA Cell Biol.* 31 (2012) 876–882.

- [34] N.H. Moghadam, S. Salehzadeh, N. Shahabadi, Spectroscopic and molecular docking studies on the interaction of antiviral drug nevirapine with calf thymus DNA, *Nucleos Nucleot. Nucleic Acids* 36 (2017) 553–570.
- [35] J.B. Chaires, N. Dattagupta, D.M. Crothers, Kinetics of the daunomycin-DNA interaction, *Biochemistry* 24 (1985) 260–267.
- [36] L.A. Marky, K.J. Breslauer, Origins of netropsin binding affinity and specificity: correlations of thermodynamic and structural data, *Proc. Natl. Acad. Sci. Unit. States Am.* 84 (1987) 4359–4363.
- [37] F.A. Taniou, J. Spychala, A. Kumar, et al., Different binding mode in AT and GC sequences for unfused-aromatic dications, *J. Biomol. Struct. Dyn.* 11 (1994) 1063–1083.
- [38] S.S. Kalanur, U. Katrahalli, J. Seetharamappa, Electrochemical studies and spectroscopic investigations on the interaction of an anticancer drug with DNA and their analytical applications, *J. Electroanal. Chem.* 636 (2009) 93–100.